Iranian Journal of Science
https://doi.org/10.1007/s40995-024-01672-2

RESEARCH PAPER

Numerical Solution of Stochastic Fractional Integro-Differential Equations: The Poly-sinc Collocation Approach

Faezeh Bahmani[1] · Ali Eftekhari[1]

Received: 16 April 2024 / Accepted: 14 June 2024

Abstract
This paper presents a polynomial sinc-based collocation method, combined with Gauss–Legendre/Newton–Cotes quadrature rules, to solve stochastic fractional integro-differential equations (SFIDEs). The method approximates the solution by applying Lagrangian polynomial interpolation at sinc collocation points and simplifies the SFIDE into a system of algebraic equations, requiring low/moderate computational efforts. The proposed method is also accompanied by an error analysis, and numerical examples are provided to demonstrate its efficiency and accuracy. In noiseless conditions, the method achieves spectral accuracy and behaves like other conventional sinc methods. Finally, the paper simulates an application of a class of these equations.

Keywords Stochastic fractional integro-differential equations · Poly-sinc collocation method · Itô integral, Brownian motion process · Error analysis

Mathematics Subject Classification 26A33 · 41A05 · 65C30 · 65D05 · 65D30 · 65M70

1 Introduction

Fractional calculus is a rapidly expanding field of research, situated at the intersection of probability, differential equations, and mathematical physics (Meerschaert and Sikorskii 2019). It provides a valuable mathematical framework for modeling complex natural phenomena in fields such as physics, engineering, biology, and others (Akbari and Navaei 2024; Bisheh-Niasar 2023). Its properties of non-linearity, memory and heredity, non-locality, multi-scaling, Sun et al. (2018); Herrmann (2011) and flexibility (see Bahloul et al. 2022 and references therein) make it an adaptable and versatile modeling framework.

Stochastic functional equations, such as stochastic differential equations, stochastic integral equations, and even higher-dimensional stochastic partial differential equations, are more effective than deterministic functional equations in modeling physical systems across various scientific domains. These equations incorporate unpredictable factors into the modeling of real-life phenomena, allowing for more accurate and consistent descriptions of such phenomena in fields such as physics, biology, finance, engineering, and chemistry. Studies have demonstrated their greater efficacy in modeling real-world systems Mao 2007; Oksendal 2013; Klebaner 2012; Stark and Woods 1986; Bhattacharya and Waymire 2009.

Solving stochastic functional equations can be challenging due to the involvement of complex mathematical operations and random variables, which often makes it difficult or impossible to find exact solutions. Various numerical methods are utilized to address this issue to obtain approximate solutions.

This paper introduces a numerical approach for solving stochastic fractional integro-differential equations (SFIDEs). The Fokker-Planck equation is a type of stochastic partial differential equation utilized to simulate particle movements that undergo Brownian motion. By incorporating fractional derivatives, it transforms into SFIDE (Denisov et al. 2009). The mathematical structure of this model can be outlined as follows:

✉ Ali Eftekhari
eftekhari@kashanu.ac.ir

Faezeh Bahmani
faezehbahmani68@gmail.com

[1] Department of Applied Mathematics, Faculty of Mathematical Sciences, University of Kashan, Kashan 87317-53153, Iran

Published online: 02 August 2024

$$D^{\gamma}_{0,t}y(t) = g(t,y(t)) + \int_0^t \mathcal{K}_1(\tau,t)y(\tau)\mathrm{d}\tau + \xi\int_0^t \mathcal{K}_2(\tau,t)y(\tau)\mathrm{d}W(\tau), \quad (1)$$

$$y(0) = \bar{y}_0, \quad (2)$$

for $t \in [0,1]$ and $0 \le \gamma \le 1$. y, g, $\mathcal{K}_1$ and $\mathcal{K}_2$ are the stochastic processes defined on a filtered probability space $(\Omega, \mathcal{F}, \mathbb{P})$ having a normal filtration indicated by $\{\mathcal{F}_t\}_{t\ge 0}$, and our numerical method seeks to determine the value of y, which is currently unknown. W is a Brownian motion process defined within the same filtered probability space and the second integral represented in (1) is of Itô type. Furthermore, g is a known process in the same space that satisfied the Lipschitz condition concerning y. ξ is maximum amplitude of noise (Ahmadi et al. 2017). Also, $\bar{y}_0$ is a real-valued constant. Here, $D^{\gamma}_{0,t}$ refers to the left fractional differential operator of order γ according to the definition of Caputo (Podulbny 1999; Saadatmandi et al. 2020),

$$D^{\gamma}_{0,t}y(t) = \frac{1}{\Gamma(m-\gamma)}\int_0^t y^{(m)}(\tau)(t-\tau)^{m-\gamma-1}\mathrm{d}\tau, \quad m-1<\gamma\le m, \quad m\in\mathbb{N}, \quad (3)$$

where $\Gamma(.)$ stands for Gamma function.

There exist several numerical methods to solve equations of this kind. Taheri et al. (2017) focused on using shifted Legendre polynomials with a spectral collocation method. The Galerkin method based on Jacobi polynomials was utilized by Kamrani (2015). Mirzaee and Samadyar (2019) developed a meshless approach that involves radial basis functions. In their latest publications, Singh and Mehra (2021) presented a Legendre wavelet collocation method and introduced a collocation method based on Muntz-Legendre polynomials (Singh and Mehra 2023). In this regard, novel research has been conducted by Mirzaee and his students, including spline-based methods (Mirzaee and Alipour 2020a, b; Mirzaee et al. 2020; Mirzaee and Alipour 2021a), moving least square schemes (Mirzaee et al. 2021; Solhi et al. 2024, 2023) and finite difference and meshfree methods (Mirzaee and Alipour 2021b). Notably, Mirzaee et al. have recently employed Floater-Hormann interpolation (Mirzaee et al. 2023) and meshless barycentric rational interpolation (Mirzaee et al. 2024) to solve SIVIEs and SFIDEs, respectively.

In the present paper, we introduce a novel and reliable collocation technique based on Lagrange polynomial approximation at non-equidistant sinc interpolation points generated by a conformal map. Sinc techniques have been recognized as a valuable tool for numerical analysis and simulation in various fields, including applied physics and engineering (Stenger 1993; Lund and Bowers 1992). The exponential convergence rate of classical sinc functions (Stenger 1993) has made them a popular choice for interpolation. However, when using the sinc interpolation formula to estimate the derivative of a function on a finite or semi-infinite interval, accuracy near the endpoints of these intervals may be poor (Stenger 1993; Lund and Bowers 1992). Overcoming this challenge was the philosophy behind the creation of interpolation polynomial approximation at sinc points, so-called poly-sinc approximation by Stenger (2009), which inspired further discussions among him and other researchers (Youssef and Baumann 2014; Youssef et al. 2016; Stenger et al. 2013). It is possible to achieve a uniformly accurate approximation of a function's derivative over a finite/infinite interval using poly-sinc approximation, as given in Stenger (2009). In addition to this feature, the poly-sinc approximation has an error of exponential order (Stenger 2009), and the estimation of its Lebesgue constant follows a logarithmic asymptotic pattern (Youssef et al. 2016). This approach has also been rated as a reliable and quite efficient way of handling ordinary differential equations with endpoint singularities (Youssef and Baumann 2014, 2015, 2019; Eftekhari 2023) and has outstanding performance in solving some fractional/stochastic differential or integral equations (Moshtaghi and Saadatmandi 2021, 2020; Youssef and Pulch 2021). These advantages, in addition to the spectral accuracy of the poly-sinc method and the convenience of performing algebraic calculations on polynomials, motivate us to use this approach in solving Equations (1)-(2). In summary, the appealing features of the investigated method include:

- Polynomial-based computations
- Spectral convergence (in deterministic cases)
- Low/moderate spectral resolution
- Problem reduction to a nonlinear system of equations
- Straightforward implementation

Our paper is organized as follows: The preliminaries of stochastic calculus and poly-sinc interpolation are presented in Sect. 2. Section 3 outlines a spectral collocation method based on poly-sinc approximation for solving fractional stochastic integro-differential equations in the form of (1). The analysis of the convergence and error of

the proposed method is performed in Sect. 4. Section 5 contains numerical experiments that demonstrate the effectiveness of our approach. Additionally, we provide an example of a real-life application of SFIDEs in section 6. Finally, we conclude our paper with a brief summary in the last section.

2 Preliminaries and Requirements

This section overviews the mathematical foundations necessary for our subsequent discussion, including stochastic calculus and poly-sinc interpolation.

2.1 Stochastic Calculus

In 1827, botanist Robert Brown observed that tiny pollen grains suspended in water move irregularly and unpredictably. This led to the formal definition of Brownian motion, considered one of the most important stochastic processes (Calin 2015).

Definition 2.1 (Klebaner 2012) A Brownian motion process is a continuous-time stochastic process $W(t)$, $t \geq 0$, that starts at the origin $(W(0) = 0, \text{with probability } 1)$ and satisfies the following properties

(i) $W(t)$ has independent increments;
(ii) $W(t)$ is a continuous function of t; and
(iii) The increments $W(t) - W(s)$ are normally distributed with mean zero and variance equal to the absolute difference between t and s, i.e., $W(t) - W(s) \sim \mathcal{N}(0, \mid t - s \mid)$.

Theorem 2.2 (*Oksendal* 2013) (*Integration by parts*) *Assuming that* $y(s, \omega) = y(s)$ *is a continuous function and of bounded variation with respect to* $s \in [0, t]$ *for almost all* ω. *Then the following property holds*

$$\int_0^t y(s)\mathrm{d}W(s) = y(t)W(t) - \int_0^t W(s)\mathrm{d}y(s). \tag{4}$$

2.2 Poly-sinc Interpolation

Assume that $u : [a, b] \to \mathbb{R}$ is a continuous function. The accuracy of the Lagrange polynomial approximation for u is dependent on the set of interpolation points $\{t_k, u(t_k)\}_{k=0}^{n}$ (Smith 2006). Equidistant points, which are the most frequently used set of points, have yielded poor results in the Lagrange polynomial approximation (Stenger et al. 2013). Alternative point sets like Chebyshev and modified Chebyshev points can improve function approximation accuracy (Smith 2006). Recent studies have demonstrated that the utilization of sinc points as interpolation points are also useful and effective (Youssef et al. 2016).

To construct the Lagrange polynomial approximation using sinc points, we will use some mathematical notation. Throughout this paper, $\mathbb{Z}$ denotes the set of all integers, and $\mathbb{R}$ and $\mathbb{C}$ stand for the real line and complex plane, respectively. We denote by $h > 0$ the mesh size associated with an evenly spaced grid $\{kh\}_{k=-N}^{N}$, where $N \in \mathbb{Z}^+$. Given that our problem is focused on a subset of the real numbers, specifically the interval $[a, b] = [0, 1]$. Therefore, we apply the conformal map

$$w = \phi(z) = \ln\left(\frac{z}{1-z}\right)$$

from the simply connected region (known as eye-shaped region) defined as

$$\mathcal{D}_E = \left\{z \in \mathbb{C} : \left|\arg\left(\frac{z}{1-z}\right)\right| < d\right\}, \tag{5}$$

to the strip-shaped region

$$\mathcal{D}_d = \{w \in \mathbb{C} : |\Im(w)| < d\}, \tag{6}$$

with a width of $2d$ where $d \in (0, \frac{\pi}{2})$. The rule of ϕ implies that $0 = \phi^{-1}(-\infty)$ and $1 = \phi^{-1}(\infty)$. The collection of separated sinc points is also defined as follows

$$t_k = \phi^{-1}(kh) = \frac{e^{kh}}{1 + e^{kh}}, \quad k = -N, \ldots, N. \tag{7}$$

Let $\mathfrak{P}_n$ be the space of polynomials having a degree no more than $n = 2N$. Now, we focus on constructing the Lagrange interpolating polynomials of degree $\leqslant n$ based on sinc points using the set of interpolation points $(t_k, u(t_k))$, where $\{t_k\}_{k=-N}^{N}$ represent sinc points obtained at (7) and $\{u_k\}_{k=-N}^{N}$ are the values of u at sinc points. The one-dimensional interpolation approximation for u on the interval [0, 1] using $n + 1$ sinc points can be expressed as

$$U_N(t) = \sum_{k=-N}^{N} u(t_k)\mathcal{L}_k(t), \tag{8}$$

where $\{\mathcal{L}_k\}_{k=-N}^{N}$ are the Lagrange basis polynomials at sinc points in the following form

$$\mathcal{L}_k(t) = \prod_{\substack{j=-N \\ j\neq k}}^{N} \frac{t-t_j}{t_k-t_j}, \quad k=-N,\ldots,N. \tag{9}$$

To effectively obtain the fractional derivative of poly-sinc interpolation and analyze errors, we follow (Moshtaghi and Saadatmandi 2021) and adopt the interpolation U_N as follows:

$$U_N(t) = \sum_{k=1}^{2N+1} u(\breve{t}_k)\breve{\mathcal{L}}_k(t), \tag{10}$$

where, $\breve{t}_k = t_{k-N-1}$ and $\breve{\mathcal{L}}_k(t)$ denotes the expansion of $\mathcal{L}_{k-N-1}(t)$ in terms of powers of t,

$$\breve{\mathcal{L}}_k(t) = \sum_{i=0}^{2N} a_{i,k}t^i, \quad k=1,\cdots,2N+1. \tag{11}$$

Similar to the regular sinc approximation, $U_N(t)$ provides a spectral accuracy in approximating the function $u(t)$ known at sinc points (Stenger 1993). However, compared to classical sinc methods, it has the privilege that it approximates $u'(t)$ uniformly on [0, 1] with an exponential accuracy (Stenger 2009).

The following convergence theorems concerning the poly-sinc approximation are presented.

Theorem 2.3 (*Stenger 2009*; *Moshtaghi and Saadatmandi 2021*) *Let the set $\mathcal{D}_E$ be defined as the inverse image of $\mathcal{D}_d$ under the conformal mapping $\phi(t) = \ln(\frac{t}{1-t})$, where $\mathcal{D}_d$ is defined in (6). Let $\mathcal{D}_2$ be the union of $\mathcal{D}_E$ with the discs $\mathcal{B}_\delta = \{z\in\mathbb{C} : |z-\delta|<\varepsilon\}$, where $\delta\in(0,1)$ and $\varepsilon>0$. If y is an analytic function that is uniformly bounded by $\mathcal{C}>0$ on $\mathcal{D}_2$, and we let $h=\frac{v}{\sqrt{N}}$, where $v>0$, and set $y_N(t)$ as defined in (8), then we can obtain a bound on the error $|y(t)-y_N(t)|$ for $t\in[0,1]$, as follows*:

$$|y(t)-y_N(t)| \le \mathcal{A}\frac{\sqrt{N}}{(2\varepsilon)^{2N}}\exp\left(\frac{-\pi^2\sqrt{N}}{2v}\right), \tag{12}$$

where $\mathcal{A}$ is a constant, independent of N.

Theorem 2.4 (*Moshtaghi and Saadatmandi 2021*) *Let y be an analytic function that is uniformly bounded on some closed disk $\mathcal{D}_3 = \{z\in\mathbb{C} : |z-1/2|<\rho,\ \rho>3/2\}$ containig the interval [0, 1]. Additionally, suppose that $0<\gamma<1$. Then, under the assumptions of Theorem 2.3, there exist constants $\mathcal{S}_\gamma>0$ and $0<\varrho<1$, independent of N, such that*

$$|D^{\gamma}_{0,t}y(t) - D^{\gamma}_{0,t}y_N(t)| \le \frac{\mathcal{S}_\gamma}{(\rho-\frac{1}{2})^{2N+2}}\left\{(2N+1)\varrho^{2N} + \frac{\sqrt{N}}{2^{2N}}\exp\left(\frac{-\pi^2\sqrt{N}}{2v}\right)\right\}. \tag{13}$$

3 Methodology Description

In this section, we utilize the poly-sinc collocation technique to solve the SFIDE Eqs. (1)-(2). For this purpose, upon choosing a fixed positive integer N and applying the poly-sinc interpolation to y, we can approximate it as follows

$$y(t) \approx y_N(t) = \sum_{i=1}^{2N+1} y_i\breve{\mathcal{L}}_i(t), \tag{14}$$

where $\{y_i := y_N(\breve{t}_i)\}_{i=1}^{2N+1}$ is a collection of unknown coefficients. Substituting (14) into Equations (1) and (2) allows us to evaluate the unknown coefficients y_i and obtain $y_N(t)$. Hence, the following equations must be imposed

$$D^{\gamma}_{0,t}y_N(t) = g(t,y_N(t)) + \int_0^t \mathcal{K}_1(\tau,t)y_N(\tau)\mathrm{d}\tau + \xi\int_0^t \mathcal{K}_2(\tau,t)y_N(\tau)\mathrm{d}W(\tau), \tag{15}$$

$$y_N(0) = \bar{y}_0. \tag{16}$$

Thanks to Theorem 2.2, with a little rewriting of the Wiener integral in (15), the aforementioned equation will get the following form

$$D^{\gamma}_{0,t}y_N(\tau) = g(t,y_N(t)) + \xi\,\mathcal{K}_2(t,t)y_N(t)W(t) + \int_0^t \mathcal{K}_1(\tau,t)y_N(\tau)\mathrm{d}\tau - \xi\int_0^t \mathfrak{K}_2(\tau,t,y_N(\tau))W(\tau)\mathrm{d}\tau, \tag{17}$$

where $\mathfrak{K}_2(\tau,t,y_N(\tau)) = \frac{\partial}{\partial\tau}(\mathcal{K}_2(\tau,t)y_N(\tau))$.

We now provide approximations for the integrals in (17) with the help of the so-called Gauss–Legendre and Newton–Cotes quadratures. Having focused on the first integral of (17), we can employ the Gauss–Legendre rule to obtain a desirable approximation. Introducing the change of variable $\eta = \frac{2\tau - t}{t}$ or $\tau = \frac{t}{2}(\eta + 1)$ for integration, gives

$$\int_0^t \mathcal{K}_1(\tau, t) y_N(\tau) \mathrm{d}\tau = \frac{t}{2} \int_{-1}^{1} \mathcal{K}_1\Big(\frac{t}{2}(\eta + 1), t\Big) y_N\Big(\frac{t}{2}(\eta + 1)\Big) \mathrm{d}\eta. \tag{18}$$

Then, using the M_1-point Gauss–Legendre quadrature rule, with the integration abscissae $\{\eta_i\}_{i=1}^{M_1}$ and weights $\{\varpi_i\}_{i=1}^{M_1}$, we obtain the following approximation for (18)

$$\int_0^t \mathcal{K}_1(\tau, t) y_N(\tau) \mathrm{d}\tau \simeq \frac{t}{2} \sum_{i=1}^{M_1} \varpi_i \mathcal{K}_1\Big(\frac{t}{2}(\eta_i + 1), t\Big) y_N\Big(\frac{t}{2}(\eta_i + 1)\Big). \tag{19}$$

We now turn to numerically approximate the second integral given in (17) using a composite Newton–Cotes quadrature, which has demonstrated its compatibility and efficiency in dealing with integrals involving non-smooth integrands (Delves and Mohamed 1985). To accomplish this method, for fixed positive integers M_2 and P, we use the M_2-point quadrature rule with P panels in the following manner:

Making the variable transformation $\theta = \frac{\tau}{t}$, for the aforementioned integration yields

$$\int_0^t \mathfrak{K}_2(\tau, t, y_N(\tau)) W(\tau) \mathrm{d}\tau = t \int_0^1 \mathfrak{K}_2(t\theta, t, y_N(t\theta)) W(t\theta) \mathrm{d}\theta. \tag{20}$$

Then, we employ the M_2-point quadrature rule with P panels to approximate the right-hand side of (20) as follows (Delves and Mohamed 1985)

$$\begin{aligned} & t \int_0^1 \mathfrak{K}_2(t\theta, t, y_N(t\theta)) W(t\theta) \mathrm{d}\theta \\ & \quad \simeq t \sum_{j=1}^{P} \sum_{k=1}^{M_2} w_k^{(j)} \mathfrak{K}_2(t\theta_k^{(j)}, t, y_N(t\theta_k^{(j)})) W(t\theta_k^{(j)}), \end{aligned} \tag{21}$$

where $\{\theta_k^{(j)}\}_{k=1}^{M_2}$ and $\{w_k^{(j)}\}_{k=1}^{M_2}$, $j = 1, ..., P$, are the quadrature nodes and weights of the closed Newton–Cotes rule, respectively.

To discretize the equation, by substituting (19) and (21) into (17), we arrive at

$$\begin{aligned} D_{0,t}^{\gamma} y_N(t) &= g(t, y_N(t)) + \xi\, \mathcal{K}_2(t, t) y_N(t) W(t) \\ &\quad + \frac{t}{2} \sum_{i=1}^{M_1} \varpi_i \mathcal{K}_1\Big(\frac{t}{2}(\eta_i + 1), t\Big) y_N\Big(\frac{t}{2}(\eta_i + 1)\Big) \\ &\quad - t \sum_{j=1}^{P} \sum_{k=1}^{M_2} w_k^{(j)} \mathfrak{K}_2(t\theta_k^{(j)}, t, y_N(t\theta_k^{(j)})) W(t\theta_k^{(j)}), \end{aligned} \tag{22}$$

where $\{\eta_i\}_{i=1}^{M_1}$, $\{\varpi_i\}_{i=1}^{M_1}$, $\{\theta_k^{(j)}\}_{k=1}^{M_2}$ and $\{w_k^{(j)}\}_{k=1}^{M_2}$, $j = 1, ..., P$, correspond to the previously defined values.

Collocating (22) at the sinc points $\{\breve{t}_r\}_{r=2}^{2N+1}$, we obtain the discrete system

$$\begin{aligned} D_{0,t}^{\gamma} y_N(\breve{t}_r) &= g(\breve{t}_r, y_N(\breve{t}_r)) + \xi\, \mathcal{K}_2(\breve{t}_r, \breve{t}_r) y_N(\breve{t}_r) W(\breve{t}_r) \\ &\quad + \frac{\breve{t}_r}{2} \sum_{i=1}^{M_1} \varpi_i \mathcal{K}_1\Big(\frac{\breve{t}_r}{2}(\eta_i + 1), \breve{t}_r\Big) y_N\Big(\frac{\breve{t}_r}{2}(\eta_i + 1)\Big) \\ &\quad - \breve{t}_r \sum_{j=1}^{P} \sum_{k=1}^{M_2} w_k^{(j)} \mathfrak{K}_2(\breve{t}_r\theta_k^{(j)}, \breve{t}_r, y_N(\breve{t}_r\theta_k^{(j)})) \\ &\quad W(\breve{t}_r\theta_k^{(j)}), \quad r = 2, \cdots, 2N + 1. \end{aligned} \tag{23}$$

An alternative equation can be derived by substituting $y_N(0)$ in the initial condition (2) as follows

$$y_N(0) = \bar{y}_0. \tag{24}$$

Let us define

$$\begin{aligned} \mathbf{y} &= (y_1, \ldots, y_{2N+1})^T, \\ H_1(\mathbf{y}) &= y_N(0) - \bar{y}_0, \\ H_r(\mathbf{y}) &= D_{0,t}^{\gamma} y_N(\breve{t}_r) - g(\breve{t}_r, y_N(\breve{t}_r)) - \xi\, \mathcal{K}_2(\breve{t}_r, \breve{t}_r) y_N(\breve{t}_r) W(\breve{t}_r) \\ &\quad - \frac{\breve{t}_r}{2} \sum_{i=1}^{M_1} \varpi_i \mathcal{K}_1\Big(\frac{\breve{t}_r}{2}(\eta_i + 1), \breve{t}_r\Big) y_N\Big(\frac{\breve{t}_r}{2}(\eta_i + 1)\Big) \\ &\quad - \breve{t}_r \sum_{j=1}^{P} \sum_{k=1}^{M_2} w_k^{(j)} \mathfrak{K}_2(\breve{t}_r\theta_k^{(j)}, \breve{t}_r, y_N(\breve{t}_r\theta_k^{(j)})) \\ &\quad W(\breve{t}_r\theta_k^{(j)}), \quad r = 2, \ldots, 2N + 1, \end{aligned}$$

and

$$\mathbf{H}(\mathbf{y}) = (H_1(\mathbf{y}), \ldots, H_{2N+1}(\mathbf{y}))^T.$$

Thus, the system of Equations (23) and (24) can be reduced to

$$\mathbf{H}(\mathbf{y}) = \mathbf{0}, \tag{25}$$

for unknown coefficients $\{y_r\}_{r=1}^{2N+1}$. The system (25) can be solved for y_r $(r = 1, \ldots, 2N + 1)$ using a suitable iterative solver such as Newton's method, ultimately yields an estimate for $y_N(t)$. In the following, we outline the algorithm for the proposed scheme.

Algorithm 1 Poly-sinc Collocation Method

Input:
Number of sample paths: $15 \leq q \leq 250$
Stochastic processes of SFIDE (1): g, $\mathcal{K}_1$, $\mathcal{K}_2$
Simulating the Brownian motion process: $W(t)$
Fractional order: γ
Positive integer for generating sinc points: N
Positive parameter associated with mesh size $h = \frac{\nu}{\sqrt{N}}$: ν
Number of nodal points for Legendre-Gauss quadrature: M_1
Number of panels for computing integral (21) of Itô type: P
Number of nodal points for closed Newton-Cotes formula: M_2
Stopping criterion for Newton's iterative method: ϵ
Maximum number of iterations for Newton's iterative method ≤ 8 with the initial guess $\mathbf{0}$.
Output:
The approximate solution after q simulations: $y(t) \approx y_N(t)$
procedure Poly-sinc Collocation
    Calculate $\breve{t}_k$, $k = 1, \ldots, 2N+1$, as sinc points.
    Calculate Lagrange basis polynomials at sinc points $\breve{L}_k$, $k = 1, \ldots, 2N+1$, defined in (11).
    Calculate η_i, $i = 0, \ldots, M_1$, as zeros of Legendre polynomial of degree $M_1 + 1$.
    Calculate weights ϖ_i, $i = 0, \ldots, M_1$, for M_1-point Legendre-Gauss quadrature rule.
    Calculate quadrature nodes $\theta_k^{(j)}$, $k = 1, \ldots, M_2$, $j = 1, \ldots, P$, and weights $w_k^{(j)}$, $k = 1, \ldots, M_2$, $j = 1, \ldots, P$, of the closed Newton-Cotes formula defined in section 3.
    Generate the system $H_i(y) = 0, i = 1, \ldots, 2N+1$ defined in section 3.
    Employ Newton's iterative method to solve (25).
end procedure

4 Error Bound and Convergence Analysis

In this section, we will present two theorems concerning numerical integration over the unit interval $[0, 1] \subset \mathbb{R}$ (Delves and Mohamed 1985), before delving into error analysis.

Theorem 4.1 (*Gauss–Legendre quadrature*) *Let $M_1 > 0$ be a fixed integer, and the function $f : [0, 1] \longrightarrow \mathbb{R}$ be sufficiently smooth. Then, the definite integral of f over* [0, 1], *denoted If, is approximated as follows*

$$If = \int_0^1 f(t)\mathrm{d}t \simeq Qf = \sum_{i=1}^{M_1} \varpi_i f(\eta_i), \tag{26}$$

where $\{\eta_i\}_{i=1}^{M_1}$ are the roots of the shifted Legendre polynomial of degree M_1 on the interval (0, 1) and $\{\varpi_i\}_{i=1}^{M_1}$ are the weights associated with the quadrature formula (26). Moreover, the error of the quadrature, $If - Qf$, denoted Ef(G-L), can be bounded by

$$|Ef(\text{G-L})| \leq \frac{2\mathcal{M}}{(2M_1 - 1)!}, \tag{27}$$

where $\mathcal{M} = \sup_{0 \leq t \leq 1} |f^{(2M_1)}(t)|$.

Theorem 4.2 *Let $M_2, P > 1$ be two fixed integers and f be a Riemann integrable function over the interval* [0, 1]. *Assume that $h = \frac{1}{P}$ and $Q_{M_2}(f; ((j-1)h, jh))$ represents the*

closed M_2-point Newton–Cotes rule approximation to the integral $\int_{(j-1)h}^{jh} f(t)\,dt$, *defined by*

$$Q_{M_2}(f;((j-1)h,jh)) = \sum_{i=1}^{M_2} w_i^{(j)} f(\theta_i^{(j)}), \quad j = 1,\cdots,P,$$

where $\theta_i^{(j)} := \frac{1}{P}\left(\frac{i-1}{M_2-1} + j - 1\right)$ and $w_i^{(j)}$ are the quadrature nodes and weights, respectively. Then, the P-panel repeated quadrature rule (Q_{M_2}) to the integral $\int_0^1 f(t)\,dt$ can be obtained as follows

$$\int_0^1 f(t)\,dt = \sum_{j=1}^{P} Q_{M_2}(f;((j-1)h,jh)) + E_{M_2,P}, \tag{28}$$

where $E_{M_2,P}$ denotes the quadrature error. Moreover, the error tends to zero as the number of panels increases, i.e.,

$$\lim_{P\to\infty} E_{M_2,P} = 0. \tag{29}$$

We are now ready to present the theory regarding the error analysis for our proposed method. In the upcoming theorem, we will seek a bound on the error utilizing the maximum function norm, as defined by

$$\|f(t)\| = \max_{0\le t\le 1} |f(t)|. \tag{30}$$

Theorem 4.3 *With the same assumptions and notation as in Theorems 2.3 and 2.4, let $y(t)$ and $y_N(t)$ denote, respectively, the exact and poly-sinc solutions of (1)-(2). Assume the additional regularity $\mathcal{K}_1(\tau,t)y(\tau) \in C^{2M_1}[0,1]$, for fixed $t \in [0,1]$, and Lipschitz continuity of g and $\mathfrak{K}_2$ in Eq. (17) with constants L_g and $L_{\mathfrak{K}_2}$, respectively. Moreover, assuming that upper bounds $\|\mathcal{K}_i\| \le R_i$ for $i = 1,2$, and $\|W\| \le G$, for some $R_i, G \in \mathbb{R}$, we can establish a constant $\mathcal{T}$ independent of N such that*

$$\begin{aligned}\|E_N(y(t))\| &\le \frac{\mathcal{M}}{(2M_1-1)!} + \frac{\mathcal{S}_\gamma}{(\rho-\frac{1}{2})^{2N+2}}(2N+1)\varrho^{2N} \\ &+ \left(\frac{3\mathcal{T}}{\varepsilon^{2N}} + \frac{\mathcal{S}_\gamma}{(\rho-\frac{1}{2})^{2N+2}}\right)\frac{\sqrt{N}}{2^{2N}}\exp\left(\frac{-\pi^2\sqrt{N}}{2v}\right) \\ &+ E_{M_2,P},\end{aligned}$$

where,

$$\begin{aligned}E_N(y(t)) &= \Lambda_1(y(t)) - \Lambda_2(y_N(t)),\\ \Lambda_1(y(t)) &= D_{0,t}^{\gamma} y(t) - g(t,y(t)) - \xi\,\mathcal{K}_2(t,t)y(t)W(t) \\ &\quad - \frac{t}{2}\int_{-1}^{1} \mathcal{K}_1\left(\frac{t}{2}(\eta+1),t\right) y\left(\frac{t}{2}(\eta+1)\right)d\eta \\ &\quad - t\int_0^1 \mathfrak{K}_2(t\theta,t,y(t\theta))W(t\theta)\,d\theta,\end{aligned} \tag{31}$$

$$\begin{aligned}\Lambda_2(y(t)) &= D_{0,t}^{\gamma} y(t) - g(t,y(t)) - \xi\,\mathcal{K}_2(t,t)y(t)W(t) \\ &\quad - \frac{t}{2}\sum_{i=1}^{M_1} \varpi_i \mathcal{K}_1\left(\frac{t}{2}(\eta_i+1),t\right) y\left(\frac{t}{2}(\eta_i+1)\right) \\ &\quad - t\sum_{j=1}^{P}\sum_{k=1}^{M_2} w_k^{(j)} \mathfrak{K}_2(t\theta_k^{(j)},t,y(t\theta_k^{(j)}))W(t\theta_k^{(j)}),\end{aligned} \tag{32}$$

where $\{\eta_i\}_{i=1}^{M_1}$, $\{\varpi_i\}_{i=1}^{M_1}$, $\{\theta_k^{(j)}\}_{k=1}^{M_2}$ and $\{w_k^{(j)}\}_{k=1}^{M_2}$, $j = 1...P$, are defined in Eqs. (19) and (21).

Proof Using triangle inequality over $\|E_N(y(t))\|$, we have

$$\begin{aligned}\|E_N(y(t))\| &\le \|\Lambda_1(y(t)) - \Lambda_2(y(t))\| \\ &\quad + \|\Lambda_2(y(t)) - \Lambda_2(y_N(t))\|.\end{aligned} \tag{33}$$

Subtracting the right-hand sides of (31) and (32), taking absolute values, and using triangle inequality again, we get

$$\begin{aligned}&|\Lambda_1(y(t)) - \Lambda_2(y(t))| \\ &\le \frac{1}{2}\left|\int_{-1}^{1} \mathcal{K}_1\left(\tfrac{t}{2}(\eta+1),t\right) y\left(\tfrac{t}{2}(\eta+1)\right)d\eta \right. \\ &\quad \left. - \sum_{i=1}^{M_1} \varpi_i \mathcal{K}_1\left(\tfrac{t}{2}(\eta_i+1),t\right) y\left(\tfrac{t}{2}(\eta_i+1)\right)\right| \\ &\quad + \frac{1}{2}\left|\int_0^1 \mathfrak{K}_2(t\theta,t,y(t\theta))W(t\theta)\,d\theta \right. \\ &\quad \left. - \sum_{j=1}^{P}\sum_{k=1}^{M_2} w_k^{(j)} \mathfrak{K}_2(t\theta_k^{(j)},t,y(t\theta_k^{(j)}))W(t\theta_k^{(j)})\right|\end{aligned} \tag{34}$$

According to Theorems 4.1 and 4.2 and also using relation (34), we obtain

$$\|\Lambda_1(y(t)) - \Lambda_2(y(t))\| \le \frac{\mathcal{M}}{(2M_1-1)!} + E_{M_2,P}. \tag{35}$$

Similarly, from (32), we have

$$
\begin{aligned}
&|\Lambda_2(y(t)) - \Lambda_2(y_N(t))| \\
&\quad \le |D^{\gamma}_{0,t} y(t) - D^{\gamma}_{0,t} y_N(\tau)| + |g(t, y(t)) - g(t, y_N(t))| \\
&\qquad + \xi |\mathcal{K}_2(t,t)||W(t)||y(t) - y_N(t)| \\
&\qquad + \frac{1}{2}|t| \sum_{i=1}^{M_1} \varpi_i \left| \mathcal{K}_1(\frac{t}{2}(\eta_i + 1), t) \right| \left| y(\frac{t}{2}(\eta_i + 1)) \right. \\
&\qquad \left. - y_N(\frac{t}{2}(\eta_i + 1)) \right| \\
&\qquad + |t| \sum_{j=1}^{P} \sum_{k=1}^{M_2} w_k^{(j)} \\
&\left| \mathfrak{K}_2(t\theta_k^{(j)}, t, y(t\theta_k^{(j)})) - \mathfrak{K}_2(t\theta_k^{(j)}, t, y_N(t\theta_k^{(j)})) \right| \left| W(t\theta_k^{(j)}) \right|
\end{aligned}
$$

The available assumptions of the theorem, combined with the utilization of Theorems 2.3 and 2.4, yield the following upper bound

$$
\begin{aligned}
&\|\Lambda_2(y(t)) - \Lambda_2(y_N(t))\| \\
&\quad \le \frac{\mathcal{S}_\gamma}{(\rho - \frac{1}{2})^{2N+2}} \left\{ (2N+1)\varrho^{2N} + \frac{\sqrt{N}}{2^{2N}} \exp\left(\frac{-\pi^2\sqrt{N}}{2v} \right) \right\} \\
&\qquad + \mathcal{A}(L_g + \xi R_2 G) \left\{ \frac{\sqrt{N}}{(2\varepsilon)^{2N}} \exp(\frac{-\pi^2\sqrt{N}}{2v}) \right\} \\
&\qquad + \mathcal{A}\frac{R_1}{2} \left\{ \frac{\sqrt{N}}{(2\varepsilon)^{2N}} \exp(\frac{-\pi^2\sqrt{N}}{2v}) \right\} \sum_{i=1}^{M_1} \varpi_i \\
&\qquad + \mathcal{A} G L_{\mathfrak{K}_2} \left\{ \frac{\sqrt{N}}{(2\varepsilon)^{2N}} \exp(\frac{-\pi^2\sqrt{N}}{2v}) \right\} \sum_{j=1}^{P} \sum_{k=1}^{M_2} w_k^{(j)} \\
&\quad \le \frac{\mathcal{S}_\gamma}{(\rho - \frac{1}{2})^{2N+2}} (2N+1)\varrho^{2N} \\
&\qquad + \left(\frac{3\mathcal{T}}{\varepsilon^{2N}} + \frac{\mathcal{S}_\gamma}{(\rho - \frac{1}{2})^{2N+2}} \right) \frac{\sqrt{N}}{2^{2N}} \exp\left(\frac{-\pi^2\sqrt{N}}{2v} \right),
\end{aligned}
\tag{36}
$$

where

$$
\mathcal{T} = \max \left\{ \mathcal{A}(L_g + \xi R_2 G), \mathcal{A}\frac{R_1}{2}, \mathcal{A} G L_{\mathfrak{K}_2} \right\}.
$$

Thus, by employing Equations (33), (35) and (36), we can achieve the desired result. □

The above Theorem implies that as $M_1, N, P \to \infty$, then $\|E_N(y(t))\| \to 0$. In fact, under appropriate smoothness assumptions on the given functions g, $\mathcal{K}_1$, $\mathcal{K}_2$ and especially the solution function y, the desirable solution of Eqs. (1) and (2), is obtainable for moderate values of M_1, M_2, P and low/moderate resolution N. However, the numerical results in the following section demonstrate the effectiveness of our method in estimating the solution, even when y is non-smooth.

5 Numerical Experiments

In this section, we present several examples from the literature to demonstrate the precision and effectiveness of our algorithm in handling SFIDEs. It is crucial to note that achieving satisfactory results with the proposed method relies on determining the parameter v experimentally for the mesh size h. We also employ the method outlined in Higham (2001) to simulate the Brownian motion $W(t)$. To accomplish this, we implement a discretization scheme for $W(t)$. We choose the step size $\Delta\varsigma = 1/\mathcal{J}$ for $\mathcal{J} \in \mathbb{Z}^+$ and define $\varsigma_j = j\Delta\varsigma$ and $W_j = W(\varsigma_j)$ where $j = 1, ..., \mathcal{J}$. Based on Definition 2.1, $W(0) = 0$ and $W_{j-1} = W_j + dW_j$, $j = 1, ..., \mathcal{J}$, where each dW_j is an independent random variable with a normal distribution in the form $\sqrt{\Delta\varsigma}\mathcal{N}(0,1)$. By performing linear spline interpolation at the given points $(\varsigma_j, W(\varsigma_j))$, $j = 1, ..., \mathcal{J}$, we obtain an estimate of the function $W(\varsigma)$. MATLAB program in reference (Higham 2001) can be utilized to generate Brownian motion.

To assess the numerical performance of our method in various numerical examples throughout this paper, we calculate the absolute error function $|y(t) - y_N(t)|$, where $y(t)$ denotes the solution (1) with $\mathcal{J} = 500$. Given that an exact solution to Eqs. (1) and (2) is generally unavailable, we employ a numerical approximation with a sufficiently small value of $\Delta\varsigma = 1/\mathcal{J}$, as suggested by Taheri et al. (2017).

In cases where an exact solution is known, we report the maximum absolute error as follows

$$
\mathbb{E}\|e_N\| = \frac{1}{q} \sum_{l=1}^{q} \max_{1 \le i \le 2N+1} |y_{Exact}(t_i, l) y_N(t_i, l)|. \tag{37}
$$

Here, $y_{Exact}(t)$ and $y_N(t)$ represent the exact and approximate solutions obtained through the proposed method, respectively. Additionally, the residual error ($RE(t)$) can be analyzed as shown below

$$
\begin{aligned}
&\mathbb{E}\|RE(t)\| \\
&\quad = \frac{1}{q} \sum_{l=1}^{q} \left| D^{\gamma}_{0,t} y_N(t, l) - g(t, y_N(t, l)) \right. \\
&\qquad - \xi\, \mathcal{K}_2(t,t) y_N(t, l) W(t) \\
&\qquad - \int_0^t \mathcal{K}_1(\tau, t) y_N(\tau, l) \mathrm{d}\tau \\
&\qquad \left. + \xi \int_0^t \mathfrak{K}_2(\tau, t, y_N(\tau, l)) W(\tau) \mathrm{d}\tau \right|,
\end{aligned}
\tag{38}
$$

where q denotes the total number of simulations, and $\mathbb{E}$ signifies the mathematical expectation. For deterministic cases, the error described in Equation (37) can be expressed in the following way

$$\|e_N\| = \max_{1 \le i \le 2N+1} |y_{Exact}(t_i) y_N(t_i)|. \tag{39}$$

Also, upon substituting the approximate solution into the original equation over the interval [0, 1], the residual error function $RE(t)$ can be obtained as

$$RE(t) = D^{\gamma}_{0,t} y_N(t) - g(t, y_N(t)) - \int_0^t \mathcal{K}_1(\tau, t) y_N(\tau) \mathrm{d}\tau - \xi \int_0^t \mathcal{K}_2(\tau, t) y_N(\tau) \mathrm{d}W(\tau). \tag{40}$$

In this study, we examine the behavior of the function $y_N(t)$ by setting $M_2 = 5$ and $P = 10$. The computations are performed on a personal computer featuring an Intel(R) Core(TM) i5-4200 CPU and 4.00 GB of RAM, utilizing Maple software version 2018, with a precision of 16 Digits.

Example 5.1 We investigate the SFIDE (Taheri et al. 2017) described by

$$D^{\gamma}_{0,t} y(t) = \frac{\Gamma(2) t^{1-\gamma}}{\Gamma(2-\gamma)} - \frac{t^3}{3} + \int_0^t \tau y(\tau) \mathrm{d}\tau + \int_0^t y(\tau) \mathrm{d}W(\tau), \quad t \in [0, 1],$$

subject to the initial condition $y(0) = 0$, where the exact solution is currently unknown.

In order to obtain a numerical solution, we have implemented the poly-sinc collocation technique outlined in Sect. 3. Using $M_1 = 4$, in Table 1, we have reported a comparison of the absolute error of our method with the spectral collocation method as described in Taheri et al. (2017), for $\mathcal{J} = 150$ and $\gamma = 0.5$. Through empirical analysis, we found that the values of v corresponding to $n = 4$ and $n = 10$ are 2.15 and 1.85, respectively. In our analysis, n and N represent the number of collocation points for our method and the method in Taheri et al. (2017), respectively. These results are based on the analysis of 200 sample paths. In Table 2, we have displayed the residual error for $\mathcal{J} = 150, n = 10$, and various values of t and γ over 15 sample paths. In addition, Fig. 1 illustrates approximate solutions to (1), (2) for $n = 10$ and different values of γ in the left panel, while the right panel shows the residual error curve corresponding to $\gamma = 0.25$. This figure highlights that small variations in the fractional order of the derivative lead to slight deviations in the solution curves. In this example, the use of a residual evaluation strategy confirms the efficacy of the proposed method.

Table 1 A comparison of absolute errors between the spectral collocation method (Taheri et al. 2017) and our proposed approach for Example 5.1

t	Present method		Method of Taheri et al. (2017)	
	$n = 4$	$n = 10$	$N = 5$	$N = 10$
0.0	0.0000	0.0000	0.0000	0.0000
0.1	0.0044	0.0001	–	–
0.2	0.0028	0.0000	0.0010	0.0002
0.3	0.0009	0.0000	–	–
0.4	0.0041	0.0022	0.0062	0.0045
0.5	0.0051	0.0007	–	–
0.6	0.0036	0.0017	0.0022	0.0019
0.7	0.0004	0.0173	–	–
0.8	0.0021	0.0295	0.0044	0.0088
0.9	0.0010	0.0170	–	–
1.0	0.0084	0.0043	0.0082	0.0069
CPU time(s)	5.074	5.553	–	–

Example 5.2 Consider the following SFIDE (Mirzaee and Samadyar 2019),

$$D^{\gamma}_{0,t} y(t) = \frac{7}{12} t^4 - \frac{5}{6} t^3 + \frac{2t^{2-\gamma}}{\Gamma(3-\gamma)} + \frac{t^{1-\gamma}}{\Gamma(2-\gamma)} + \int_0^t (t+\tau) y(\tau) \mathrm{d}\tau + \int_0^t \tau y(\tau) \mathrm{d}W(\tau), \quad t \in [0, 1],$$

supplemented with the initial condition $y(0) = 0$. The exact solution to this problem is unknown.

Our numerical findings are based on the values $M_1 = 4$ and $\mathcal{J} = 150$. In Table 3, we have presented the results obtained through 200 sample paths for three different values of $\gamma (= 0.25, 0.5, 0.75)$ with $n = 2, 4$, under the condition $v = 2.15$. In addition, we have reported the residual error of our method with $n = 10$ and the aforementioned values of γ in Table 4. The data in Table 4 is based on the choice of $v = 1.55$ and over 15 sample paths.

Table 2 The residual errors of Example 5.1 for $n = 10$ at various values of t and γ

t / v	$\gamma = 0.15$ 1.50	$\gamma = 0.25$ 1.55	$\gamma = 0.5$ 1.55	$\gamma = 0.75$ 1.55	$\gamma = 0.95$ 1.55
0.0	0.0000	0.0000	0.0000	0.0000	0.0000
0.1	0.0011	0.0000	0.0005	0.0053	0.0073
0.2	0.0000	0.0000	0.0000	0.0000	0.0000
0.3	0.0031	0.0128	0.0004	0.0295	0.0143
0.4	0.0024	0.0135	0.0300	0.0386	0.0307
0.5	0.0003	0.0000	0.0000	0.0000	0.0004
0.6	0.0831	0.0472	0.0092	0.0651	0.0685
0.7	0.0194	0.0116	0.0297	0.0046	0.0277
0.8	0.0079	0.0000	0.0013	0.0002	0.0005
0.9	0.0241	0.0109	0.0521	0.0231	0.0001

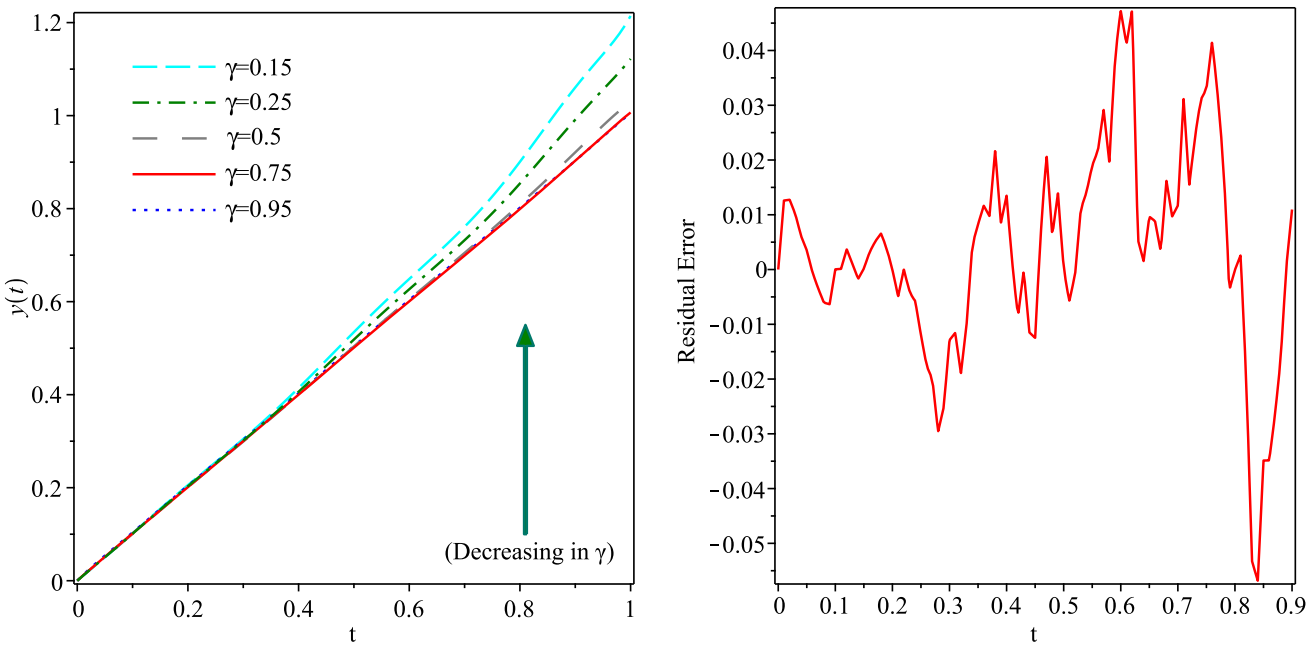

Fig. 1 Approximate solutions for various values of γ (Left) and the residual error at $\gamma = 0.25$ (Right) in Example 5.1

Table 3 The results of Example 5.2 for various values of t, γ, and $n = 2, 4$

t	$n = 2$			$n = 4$		
	$\gamma = 0.25$	$\gamma = 0.5$	$\gamma = 0.75$	$\gamma = 0.25$	$\gamma = 0.5$	$\gamma = 0.75$
0.0	1.70e−16	−1.69e−16	−9.68e−16	−4.25e−16	1.04e−14	−3.11e−14
0.1	0.0184	0.0387	0.0471	0.1066	0.1062	0.1056
0.2	0.0989	0.1247	0.1334	0.2399	0.2380	0.2361
0.3	0.2415	0.2579	0.2590	0.3973	0.3926	0.3889
0.4	0.4462	0.4382	0.4239	0.5819	0.5708	0.5636
0.5	0.7131	0.6658	0.6280	0.8030	0.7774	0.7629
0.6	1.0420	0.9405	0.8714	1.0757	1.0211	0.9919
0.7	1.4331	1.2625	1.1540	1.4209	1.3143	1.2588
0.8	1.8862	1.6316	1.4759	1.8656	1.6735	1.5741
0.9	2.4015	2.0479	1.8371	2.4426	2.1189	1.9512
1.0	2.9787	2.5114	2.2374	3.1905	2.6744	2.4063
CPU time(s)		3.410			3.683	

Table 3 demonstrates that an increase in γ corresponds to a decrease in y. Moreover, Table 4 shows that our method is reliable, as evidenced by the residual error data.

Example 5.3 Consider the SFIDE (1) with the following data (Singh and Mehra 2023)

$$g(t, y(t)) = \frac{2t^{2-\gamma}}{\Gamma(3-\gamma)} - \frac{t^6}{5}, \quad \mathcal{K}_1(\tau, t) = t\tau^2, \quad \mathcal{K}_2(\tau, t) = \tau^3,$$

along with the initial condition $y(0) = 0$.

For $\xi = 0$ and for each $0 < \gamma \leq 1$, the exact solution is t^2. Using the method described in Sect. 3, this problem is solved with the parameters $n = 2$, $M_1 = 2$, $\gamma = 0.75$, $\mathcal{J} = 150$ and $\nu = \ln(2)$. As shown in Example 6.2 of Singh and Mehra (2023), our approach demonstrates superior accuracy and faster convergence rates for deterministic problems compared to the numerical scheme presented there. The estimation for $y(t)$ can be represented as follows:

$$y(t) \approx y_1(t) = y_1\breve{\mathcal{L}}_1(t) + y_2\breve{\mathcal{L}}_2(t) + y_3\breve{\mathcal{L}}_3(t). \tag{41}$$

To obtain $\{y_i\}_{i=1}^3$, we need to use the methodology described in Sect. 3 to compute $\{\breve{\mathcal{L}}_i\}_{i=1}^3$. Given the initial condition $y(0) = 0$ and the properties of the Caputo fractional derivative operator, we can obtain the following equation

Table 4 Residual errors in Example 5.2 for different values of t and γ, with $n = 10$

t	$\gamma = 0.25$	$\gamma = 0.5$	$\gamma = 0.75$
0.0	0	0	0
0.1	0.0025	0.0023	0.0066
0.2	0.0000	0.0000	0.0000
0.3	0.0140	0.0061	0.0109
0.4	0.0415	0.0166	0.0262
0.5	0.0004	0.0002	0.0000
0.6	0.0868	0.0090	0.0551
0.7	0.0271	0.0066	0.1086
0.8	0.0038	0.0000	0.0007
0.9	0.0292	0.0249	0.0152

$$6y_1 - 8y_2 + 3y_3 = 0. \tag{42}$$

Furthermore, by collocating Eq. (22) at the points $t = 0.1, 0.5$, we can derive two additional equations:

$$\begin{aligned} &-11.24198358654720y_1 + 18.76138775150043y_2 \\ &\quad - 7.519437498286546y_3 - 0.09926542902028446 = 0, \\ &-6.140202916620419y_1 + 6.677569848433729y_2 \\ &\quad - 0.7390586868632010 - 0.5582002651470500y_3 = 0. \end{aligned} \tag{43}$$

By solving Eqs. (42) and (43), one finds

$$\begin{aligned} &y_1 = 0.1111111111111268,\ y_2 = 0.2500000000000481, \\ &y_3 = 0.4444444444445414. \end{aligned} \tag{44}$$

Using Eq. (41), we can derive the value of $y(t)$ using the following approximation

$$y(t) \approx (-5.0 \times 10^{-14})\, t + 1.000000000000293\, t^2.$$

Finally, Fig. 2 demonstrates solutions for different values of ξ with $n = 10$. As such, it is anticipated that as ξ increases, the behavior of the solution will become less predictable and display a more random pattern.

Example 5.4 We assume the SFIDE given by Singh and Mehra (2021)

$$\begin{aligned} D^{\gamma}_{0,t} y(t) = &-\frac{t^5 e^t}{5} + \frac{6t^{3-\gamma}}{\Gamma(4-\gamma)} \\ &+ \int_0^t e^t \tau y(\tau) \mathrm{d}\tau + \xi \int_0^t e^t \tau y(\tau) \mathrm{d}W(\tau), \quad t \in [0,1], \end{aligned} \tag{45}$$

with the initial condition $y(0) = 0$.

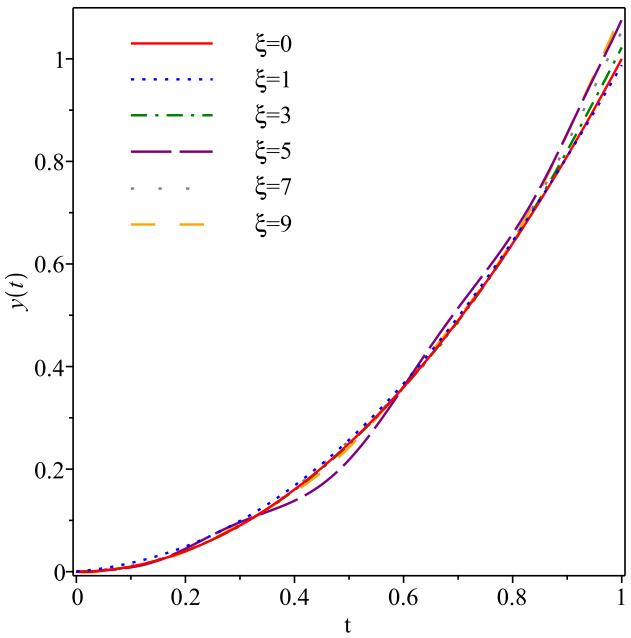

Fig. 2 Graphical representation of the solutions with $n = 10$ for various values of ξ in Example 5.3

As far as the authors know, no exact solution to this problem is currently available. However, it has been confirmed that in the deterministic case, the cubic function $y(t) = t^3$ satisfies equation (45) and its initial condition for all $0 \le \gamma \le 1$. Similar to the previous example, by choosing $\gamma = 0.75$, $n = 4$, $M_1 = 2$ and for $v = 2.15$, we can obtain a good approximation to the exact solution t^3. In Fig. 3 we

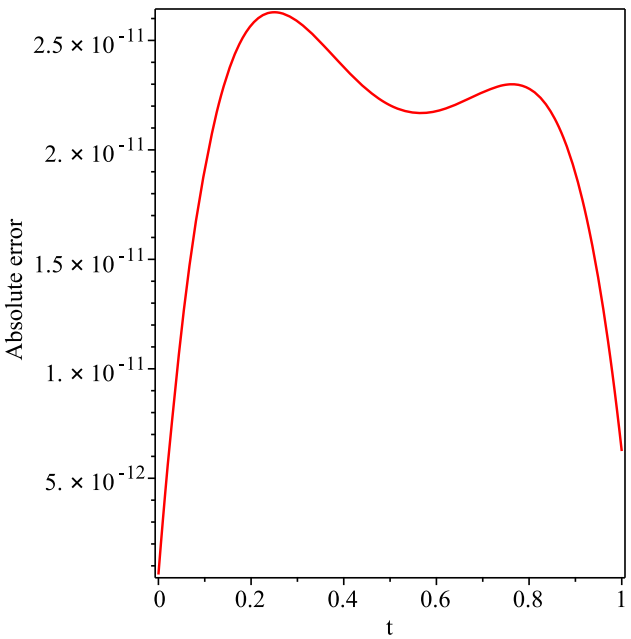

Fig. 3 The graph of the absolute error of Example 5.4, in the deterministic case, for $N = 2$, $M_1 = 2$ and $\gamma = 0.75$

Table 5 A comparison of absolute errors between the spectral collocation method (Taheri et al. 2017) and our proposed approach for Example 5.4 with $\gamma = 0.75$ and $\xi = 1$

t	Present method		Method of Taheri et al. (2017)	
	$n = 4$	$n = 10$	$N = 5$	$N = 10$
0.0	0.0000	0.0000	0.0000	0.0000
0.1	0.0019	0.0009	–	–
0.2	0.0017	0.0029	0.0034	0.0005
0.3	0.0008	0.0040	–	–
0.4	0.0001	0.0139	0.0015	0.0002
0.5	0.0001	0.0212	–	–
0.6	0.0000	0.0002	0.0047	0.0008
0.7	0.0003	0.0173	–	–
0.8	0.0020	0.0070	0.0026	0.0036
0.9	0.0069	0.0022	–	–
1.0	0.0172	0.0137	0.0066	0.0002

have shown the curve of the absolute error function $|y_N(t) - y_{Exact}(t)|$. Also, by choosing $\xi = 1$ and $\mathcal{J} = 150$, we have compared absolute errors obtained from our method and the spectral collocation technique (Taheri et al. 2017) in Table 5.

Example 5.5 We consider the following SFIDE (Taheri et al. 2017; Kamrani 2015)

$$D_{0,t}^{1/2} y(t) + y(t) = t^2 + 2\frac{t^{1.5}}{\Gamma(2.5)} + \int_0^t \tau \mathrm{d}W(\tau), \quad t \in [0, 1],$$

along with the initial condition $y(0) = 0$.

The present method is employed to find a solution for the aforementioned stochastic fractional integro-differential equation. In Table 6, we compare the numerical solutions obtained using our suggested method with those obtained through the Galerkin scheme (Kamrani 2015) and the spectral collocation method (Taheri et al. 2017), for specific values of t and n. We use $M_1 = 4$ and empirically find that for $n = 4$ and $n = 10$, the corresponding values of v are 3.24 and 3.05, respectively. The data shows that our approach offers similar or even greater accuracy compared to previous methods.

Example 5.6 Consider the SFIDE given in (1–2), with the following data (Maleknejad et al. 2012):

$g(t, y(t)) = \frac{1}{12}$, $\bar{y}_0 = 0$, the kernel functions are defined as $\mathcal{K}_1(\tau, t) = \cos(\tau)$ and $\mathcal{K}_2(\tau, t) = \sin(\tau)$, and the exact solution is given by

$$y(t) = \frac{1}{12}\exp\Big(-\frac{t}{4} + \sin(t) + \frac{\sin(2t)}{8} + \int_0^t \sin(\tau)\mathrm{d}W(\tau)\Big).$$

Table 7 presents a comparison between our method and the method of Maleknejad et al. (2012) in terms of the mean of error and the standard deviation of error with varying numbers of simulations. Here, we set $M_1 = 4$ and $\mathcal{J} = 150$. Additionally, we have included the upper and lower bounds of the 95% confidence interval in Table 7. In this example, our method utilizes five basis functions for an approximate solution, while the method in Maleknejad et al. (2012) uses eight basis functions. Therefore, the present method strikes a favorable balance between accuracy and computational cost.

Example 5.7 In this example, we consider the SFIDE with the following data (Singh and Mehra 2021): $g(t, y(t)) = \frac{t^2}{2} + \frac{\Gamma(2)}{\Gamma(2-\gamma)}$, where the kernel functions are defined as $\mathcal{K}_1(\tau, t) = 1$ and $\mathcal{K}_2(\tau, t) = 0$, and the initial condition is $y(0) = 0$, for $0 \le t \le 1$. Upon mathematical

Table 6 A comparative analysis of absolute errors using the Galerkin method (Kamrani 2015), Spectral collocation method (Taheri et al. 2017), and our approach in Example 5.5

t	Present method		Method of Taheri et al. (2017)		Galerkin Kamrani (2015)	
	$n = 4$	$n = 8$	$N = 4$	$N = 8$	$N = 4$	$N = 8$
0.01	0.0000	0.0000	0.0008	0.0003	0.0041	0.1200
0.08	0.0003	0.0000	0.0022	0.0005	0.0034	0.0025
0.16	0.0011	0.0000	0.0006	0.0018	0.0009	0.0038
0.30	0.0026	0.0019	0.0061	0.0037	0.0061	0.0086
0.43	0.0031	0.0027	0.0061	0.0048	0.0153	0.0077
0.55	0.0026	0.0012	0.0030	0.0024	0.0253	0.0031
0.63	0.0019	0.0039	0.0012	0.0000	0.0325	0.0016
0.78	0.0008	0.0013	0.0019	0.0007	0.0459	0.0139
0.84	0.0009	0.0012	0.0035	0.0027	0.0516	0.0199
0.94	0.0028	0.0000	0.0046	0.0035	0.0581	0.0315
1.00	0.0053	0.0037	0.0016	0.0009	0.0617	0.0402
CPU time(s)	3.665	3.923	–	–	–	–

Table 7 Mean, standard deviation, and 95% mean confidence intervals for error exhibited for our method versus method (Maleknejad et al. 2012)

q	$\bar{X}_E$		S_E		95% Confidence interval for mean of E				
	Present method	Method of Maleknejad et al. (2012)	Present method	Method of Maleknejad et al. (2012)	Lower present method	Upper present method	Lower method of Maleknejad et al. (2012)	Upper method of Maleknejad et al. (2012)	CPU time(s)
30	0.00581794	0.00788410	0.00345348	0.00297687	0.00481993	0.00681595	0.00681884	0.00894936	0.465
50	0.00236083	0.00793958	0.00215177	0.00340213	0.00173900	0.00298266	0.00699656	0.00888261	0.792
75	0.00568736	0.00848855	0.00635024	0.00331070	0.00385222	0.00752250	0.00773927	0.00923784	1.964
100	0.00415484	0.00838714	0.00500041	0.00341973	0.00270979	0.00559989	0.00771687	0.00905740	1.793
125	0.00296436	0.00837599	0.00295781	0.00333239	0.00210960	0.00381912	0.00779179	0.00896018	2.467
200	0.00694715	0.00833360	0.00824089	0.00363129	0.00456565	0.00932865	0.00783033	0.00883687	4.149
250	0.00828326	–	0.00649089	–	0.00640749	0.0101590	–	–	4.356

Table 8 A comparison of maximum absolute error from the method of Singh and Mehra (2021) and our proposed approach for Example 5.7

n	Present method	Method of Singh and Mehra (2021)
6	1.97e−7	1.95e−2
12	4.25e−16	4.8e−3
24	2.62e−34	1.2e−3
48	8.70e−36	2.92e−4

verification, it is evident that for $\gamma = 0$, the exact solution is $2e^t - (2 + t)$.

In Table 8, we compare the maximum absolute error of our method to the wavelet collocation method described in Singh and Mehra (2021) for different values of $n = 2N$, having set $M_1 = 10, 11$. Figure 4 displays the natural logarithm of $\|e_N\|$ versus n, and we observe that the graph has a straight-line shape, indicating that our method achieves exponential convergence under deterministic conditions. These results demonstrate the superior accuracy of our methodology, particularly in this deterministic example.

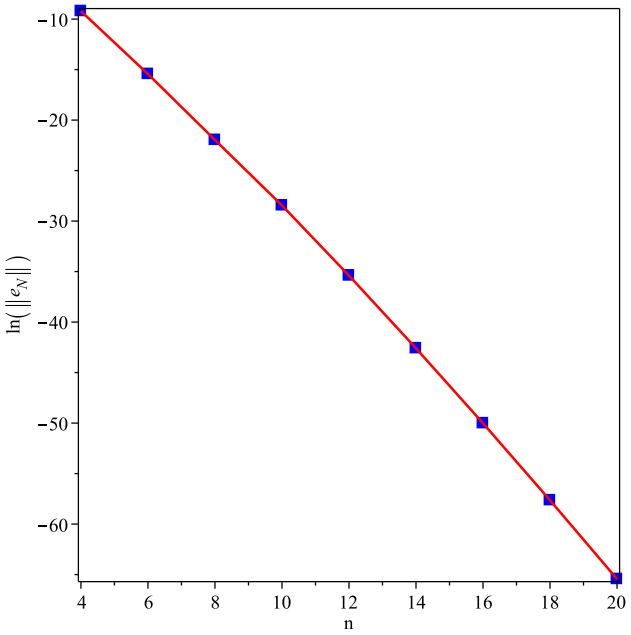

Fig. 4 Graph of the logarithm of $\|e_N\|$ for different values of $n(= 4 : 2 : 20)$

6 An Application

In this section, we revisit the Black-Scholes-Merton (BSM) model, commonly known as the Black-Scholes model. This mathematical equation is a fundamental concept in modern financial theory and helps calculate the theoretical value of derivatives. It considers various investment instruments, time, and other risk factors to determine the value of options contracts. The model was originally developed in 1973 by economists Black and Scholes (1973), along with Robert Merton, and is still widely recognized as one of the most effective methods for pricing options contracts. The model represents a specific instance of stochastic fractional integro-differential equations and is formulated as follows.

Let $y(t)$ denote the stock price at time t. We model $y(t)$ as satisfying the stochastic differential equation

$$\mathrm{d}y(t) = y(t)(\mu(t)\mathrm{d}(t) + \sigma(t)\mathrm{d}W(t)). \tag{46}$$

In this equation, $\mu(t)$ and $\sigma(t)$ are functions denoting the expected return and volatility of the stock, respectively. The term $W(t)$ denotes a Wiener process, which is a mathematical model used to describe the random

Table 9 Error mean, $\bar{X}_E$, error standard deviation, S_E, and 95% confidence interval for error mean of Black-Scholes model when $n = 10$

q	$\bar{X}_E$	S_E	95% Confidence interval for mean of E	
			Lower	Upper
30	0.0574367	0.0307497	0.0514396	0.0634338
50	0.0203446	0.0246749	0.0155323	0.0251569
100	0.0308627	0.0207296	0.0268199	0.0349055

movements of a stock price. However, the Wiener process has some limitations. It can have negative values, and it cannot be directly used for modeling stock price movements. To account for this, the term $\sigma y(t)\mathrm{d}W(t)$ is used in the equation to represent the uncertainty or unpredictability of the stock price movements. The volatility parameter σ is a positive value that indicates the extent of random fluctuations in the stock price.

Upon integrating the equation (46), we get

$$y(t) = y_0 + \int_0^t \mu(\tau)y(\tau)\mathrm{d}(\tau) + \int_0^t \sigma(\tau)y(\tau)\mathrm{d}B(\tau),$$

where y_0 represents the spot price at time 0. This integral equation is an instance of a class of equations known as Stochastic Financial Integral Differential Equations. The exact solution to the problem is

$$y(t) = y_0\exp\Big(\int_0^t \Big(\mu(\tau) - \frac{1}{2}\sigma^2(\tau)\Big)\mathrm{d}(\tau) + \int_0^t \sigma(\tau)\mathrm{d}B(\tau)\Big).$$

Table 9 reports numerical results for $M_1 = 4$ and $\mathcal{J} = 150$, assuming $\sigma = 0.1$, $\mu = 0.1$, and $y_0 = 1$.

7 Conclusion

A numerical technique for solving stochastic fractional integro-differential equations (SFIDEs) has been proposed in this paper. The technique involves using the poly-sinc collocation approach, which converts the SFIDE into a linear/nonlinear system of algebraic equations of dimension $2N + 1$ that can be easily solved by employing an appropriate iterative solver, such as Newton's method. It is worth mentioning that the deterministic and Itô integral terms in (1), have been approximated using Gauss–Legendre and P-panel, M-point Newton–Cotes quadratures, respectively. The numerical results obtained in section 5 reveal that the method attains a satisfactory solution across a diverse range of parameters, particularly for small values of N and with moderate computational efforts. In the absence of an exact solution as a reference solution, we have effectively either compared our results with previously available data or utilized a residual error approach. In summary, it is important to note that the method is straightforward to implement, exhibits rapid convergence, especially under deterministic cases, and is well-suited for addressing a wide variety of problems involving SFIDEs. However, for problems with stochastic outputs, the computed solution exhibits a smooth behavior with oscillatory patterns. Nevertheless, within its domain, the error does not experience significant growth. Lastly, our proposed methodology could employ a generalized poly-sinc collocation approach to address analogous problems in future academic research.

Acknowledgements The authors would like to thank the anonymous reviewers for their insightful comments and suggestions, which greatly improved the quality of this manuscript.

Funding This article is not supported by any funding or financial assistance.

Declarations

Conflict of interest The authors declared that they have no conflict of interest.

References

Ahmadi N, Vahidi AR, Allahviranloo T (2017) An efficient approach based on radial basis functions for solving stochastic fractional differential equations. Mathe Sci 11:113–118. https://doi.org/10.1007/s40096-017-0211-7

Akbari R, Navaei L (2024) Optimal control and stability analysis of a fractional order mathematical model for infectious disease transmission dynamics. Math Interdisc Res 9(2):199–213. https://doi.org/10.22052/MIR.2023.253000.1410

Bahloul MA, Aboelkassem Y, Laleg-Kirati MA (2022) Human hypertension blood flow model using fractional calculus. Front Physiol 13:838593. https://doi.org/10.3389/fphys.2022.838593

Bhattacharya RN, Waymire EC (2009) Stochastic processes with applications. Soc Indus Appl Math

Bisheh-Niasar M (2023) The effect of the Caputo fractional derivative on polynomiography. Math Interdisc Res 8(4):347–358. https://doi.org/10.22052/MIR.2022.246736.1367

Black F, Scholes M (1973) The pricing of options and corporate liabilities. J Polit Econ 81:637–659. https://doi.org/10.1086/260062

Calin O (2015) An informal introduction to stochastic calculus with applications. World Scientific Publishing Company, Singapore

Delves LM, Mohamed JL (1985) Computational methods for integral equations, CUP Archive

Denisov SI, Ha nggi P, Kantz H, (2009) Parameters of the fractional Fokker-Planck equation. Europhysics Lett 85(4):40007

Eftekhari A (2023) Spectral poly-sinc collocation method for solving a singular nonlinear BVP of reaction-diffusion with Michaelis–Menten kinetics in a catalyst/biocatalyst. Iran J Math Chem 14(2):77–96

Herrmann R (2011) Fractional calculus: an introduction for physicists. World Scientific Publishing Company, Singapore

Higham DJ (2001) An algorithmic introduction to numerical simulation of stochastic differential equations. SIAM Rev 43(3):525–546. https://doi.org/10.1137/S0036144500378302

Kamrani M (2015) Numerical solution of stochastic fractional differential equations. Numer Algorithms 68:81–93. https://doi.org/10.1007/s11075-014-9839-7

Klebaner FC (2012) Introduction to stochastic calculus with applications. World Scientific Publishing Company, Singapore

Lund J, Bowers KL (1992) Sinc methods for quadrature and differential equations. SIAM, Philadelphia

Maleknejad K, Khodabin M, Rostami M (2012) Numerical solution of stochastic Volterra integral equations by a stochastic operational matrix based on block pulse functions. Math Comput Model 55(3–4):791–800. https://doi.org/10.1016/j.mcm.2011.08.053

Mao X (2007) Stochastic differential equations and applications. Elsevier, Netherlands

Meerschaert MM, Sikorskii A (2019) Stochastic models for fractional calculus, vol 43. Walter de Gruyter GmbH & Co KG, Berlin

Mirzaee F, Samadyar N (2019) On the numerical solution of fractional stochastic integro-differential equations via meshless discrete collocation method based on radial basis functions. Eng Anal Bound Elements 100:246–255

Mirzaee F, Alipour S (2020) An iterative algorithm for solving two dimensional nonlinear stochastic integral equations: a combined successive approximations method with bilinear spline interpolation. Appl Math Comput 371:124947. https://doi.org/10.1016/j.amc.2019.124947

Mirzaee F, Alipour S (2020) An efficient cubic Bspline and bicubic Bspline collocation method for numerical solutions of multidimensional nonlinear stochastic quadratic integral equations. Math Methods Appl Sci 43(1):384–391. https://doi.org/10.1002/mma.5890

Mirzaee F, Rezaei S, Samadyar N (2020) Cubic B-spline approximation for linear stochastic integro-differential equation of fractional order. J Comput Appl Math 366:112440. https://doi.org/10.1016/j.cam.2019.112440

Mirzaee F, Alipour S (2021) Quintic B-spline collocation method to solve n-dimensional stochastic Itô-Volterra integral equations. J Comput Appl Math 384:113153. https://doi.org/10.1016/j.cam.2020.113153

Mirzaee F, Alipour S (2021) Numerical solution of two-dimensional stochastic time-fractional Sine–Gordon equation on non-rectangular domains using finite difference and meshfree methods. Eng Anal Boundary Elem 127:53–63. https://doi.org/10.1016/j.enganabound.2021.03.009

Mirzaee F, Solhi E, Naserifar S (2021) Approximate solution of stochastic Volterra integro-differential equations by using moving least squares scheme and spectral collocation method. Appl Math Comput 410:126447. https://doi.org/10.1016/j.amc.2021.126447

Mirzaee F, Naserifar S, Solhi E (2023) Accurate and stable numerical method based on the Floater-Hormann interpolation for stochastic Itô-Volterra integral equations. Numer Algorithms 94(1):275–292. https://doi.org/10.1007/s11075-023-01500-5

Mirzaee F, Naserifar S, Solhi E (2024) Meshless Barycentric rational interpolation method for solving nonlinear stochastic fractional integro-differential equations. Iran J Sci 1–25. https://doi.org/10.1007/s40995-024-01621-z

Moshtaghi N, Saadatmandi A (2020) Numerical solution for diffusion equations with distributed-order in time based on Sinc–Legendre collocation method. Appl Comput Math 19(3):317–335

Moshtaghi N, Saadatmandi A (2021) Polynomial-Sinc collocation method combined with the Legendre–Gauss quadrature rule for numerical solution of distributed order fractional differential equations. RACSAM. https://doi.org/10.1007/s13398-020-00976-3

Oksendal B (2013) Stochastic differential equations: an introduction with applications. Springer Science & Business Media, Berlin

Podulbny I (1999) Fractional differential equations. Academic Press, New York

Saadatmandi A, Khani A, Azizi MR (2020) Numerical calculation of fractional derivatives for the sinc functions via Legendre polynomials. Math. Interdisc. Res. 5:71- 86. https://doi.org/10.22052/mir.2018.96632.1074

Singh AK, Mehra M (2021) Wavelet collocation method based on Legendre polynomials and its application in solving the stochastic fractional integro-differential equations. J Comput Sci 51:101342. https://doi.org/10.1016/j.jocs.2021.101342

Singh AK, Mehra M (2023) An algorithm to estimate parameter in Müntz-Legendre polynomial approximation for the numerical solution of stochastic fractional integro-differential equation. J Appl Math Comput 69(3):2675–2694. https://doi.org/10.1007/s12190-023-01850-2

Smith SJ (2006) Lebesgue constants in polynomial interpolation. Ann Math Inform 33:109–123

Solhi E, Mirzaee F, Naserifar S (2023) Approximate solution of two dimensional linear and nonlinear stochastic Itô-Volterra integral equations via meshless scheme. Math Comput Simul 207:369–387. https://doi.org/10.1016/j.matcom.2023.01.009

Solhi E, Mirzaee F, Naserifar S (2024) Enhanced moving least squares method for solving the stochastic fractional Volterra integro-differential equations of Hammerstein type. Numer Algorithms 95(4):1921–1951. https://doi.org/10.1016/j.amc.2021.126447

Stark HJ, Woods JW (eds) (1986) Probability, random processes, and estimation theory for engineers. Prentice-Hall, Inc., New Jersey

Stenger F (1993) Numerical Methods Based on Sinc and Analytic Functions. Springer-Verlag, New York

Stenger F (2009) Polynomial function and derivative approximation of Sinc data. J. Complexity 25:292–302. https://doi.org/10.1016/j.jco.2009.02.010

Stenger F, Youssef M, Niebsch J (2013) Improved approximation via use of transformations. In: Analysis Multiscale Signal, Modeling, (eds) X. Shen and A. I, Zayed, NewYork, Springer

Sun H, Zhang Y, Baleanu D, Chen W, Chen Y (2018) A new collection of real world applications of fractional calculus in science and engineering. Commun Nonlinear Sci Numer Simul 64:213–231. https://doi.org/10.1016/j.cnsns.2018.04.019

Taheri Z, Javadi S, Babolian E (2017) Numerical solution of stochastic fractional integro-differential equation by the spectral collocation method. J Comput Appl Math 321:336–347. https://doi.org/10.1016/j.cam.2017.02.027

Youssef M, Baumann G (2014) Solution of nonlinear singular boundary value problems using polynomial-sinc approximation. Commun Fac Sci Univ Ank Series A1 63(2):41–58

Youssef M, Baumann G (2015) Solution of Lane–Emden type equations using polynomial-sinc collocation method. Int Sc Jr Jr Math 2(1)

Youssef M, El-Sharkawy HA, Baumann G (2016) Lebesgue constant using sinc points. Adv Numer Anal. https://doi.org/10.1155/2016/6758283

Youssef M, Baumann G (2019) Troesch's problem solved by Sinc methods. Math Comput Simul 162:31–44. https://doi.org/10.1016/j.matcom.2019.01.003

Youssef M, Pulch R (2021) Poly-Sinc solution of stochastic elliptic differential equations. J Sci Comput 87(3):1–19. https://doi.org/10.1007/s10915-021-01498-9